Blade design and performance testing of a small wind turbine rotor for low wind speed applications

Ronit. K. Singh and M. Rafiuddin Ahmed*
Division of Mechanical Engineering
The University of the South Pacific, Laucala Campus, Suva, Fiji

---

Abstract

Small wind turbines operating at low wind speeds regularly face the problem of poor performance due to laminar separation and laminar separation bubbles on the blades. This is due to the low Reynolds number (Re) resulting from low wind speeds and small rotor size. The use of specially designed low *Re* airfoils permits start up at lower wind speeds, increasing the startup torque and thus improving the overall performance of the turbine. A new airfoil was designed and the performance of a 2-bladed rotor designed for low *Re* application fitted to an Air-X marine 400 W wind turbine was tested at a wind speed range of 3 – 6 m/s. The low *Re* rotor incorporated taper and twist to the low *Re* AF300 airfoil section. The pitch of the blades was varied over a range of 15°, 18° and 20° to study the performance and the startup wind speed. It was found that the turbine performed best at 18° pitch angle. On an average, the wind turbine yielded a power coefficient (C_P) of 0.255 at a height of 8.22 m at a wind speed of 6 m/s at 18° pitch angle. Maximum C_P based on 10 sec data at the freestream velocity of 6 m/s was 0.291. The cut-in wind speed based on 10 sec averaged data at the optimum pitch angle was 3.24 m/s whereas the instantaneous cut-in wind speed was 2.34 m/s. In comparison with the baseline 3-bladed rotor, the new 2-bladed rotor produced more electrical power at the same freestream velocity.

Keywords: small wind turbine; low Reynolds number airfoil; laminar separation; power coefficient; cut-in wind speed.

---

1. Introduction

1.1 Small wind turbines

Growing awareness of rising levels of greenhouse gases [1], global warming and increasing prices of fossil fuels have led to a shift towards investing into low-cost small wind turbines. Simple structured, compact in design, portable and low noise [2], the small wind turbines are now vital wind power extracting devices in the rural, suburban and even in the populated city areas where installation of large scale wind turbines would not be accepted due to space constraints and generation of noise. Small wind turbines achieve power coefficients of 0.25 or greater in comparison to large turbines which have C_p values around 0.45 [3]. Small wind turbines have been integrated on domestic house roof tops, farms, remote communities and boats [4]. In contrast to larger horizontal axis wind turbines (HAWTs) that are located in areas dictated by optimum wind conditions, small wind turbines are required to produce power without necessarily the best of wind conditions [4-6]. A small wind turbine is one that relies on aerodynamic forces to startup and has a tail vane for passive yawing. Small wind turbines are categorized as micro (1 kW), mid-range (5 kW) and mini wind turbines (20 kW+) [7]. A more detailed description of micro wind turbines is given by Cooper as being rated less than 2.5 kW and commercially produces power in the range of 0.4 kW – 1.5 kW at 12.5 m/s wind speed [1, 8].

1.2 Laminar separation bubble

Small wind turbines operate within 100 m above sea level where the lowest portion of planetary boundary layer (PBL) is found. Within the PBL, the laminar airflow is made turbulent and slowed down by obstacles and topology [4,5,8]. Due to their small rotor size and low wind speeds; small wind turbines operating at low Reynolds numbers suffer from laminar separation bubble [3,9,10]. Laminar separation bubble is a phenomenon associated with low Reynolds number where laminar flow separates before it can transit to turbulent flow as a result of adverse pressure gradient (APG) [11]. The separated laminar flow gets re-energized and reattaches back to the surface as turbulent flow forming the so-called separation bubble. The separation bubble leads to an increase in the boundary layer thickness above it, causing excessive increase in pressure drag, a loss in aerodynamic lift and

noise [7,11,12]. Separation bubble degrades the overall aerodynamic performance of an airfoil resulting in the reduction of a turbine's startup and power coefficient [4].

1.3 Low Reynolds number airfoils for small wind turbines

Low *Re* airfoils operate below *Re* = 500,000 [10,13,14] where the flow across the upper surface of the airfoil is predominantly laminar. Airfoils within this *Re* range suffer from laminar separation bubble and are susceptible to laminar flow separation that occurs when the separated laminar boundary layer does not reattach to the surface downstream, resulting in a loss in aerodynamic performance. Low *Re* airfoils suited for small wind turbine applications must be designed to avoid high leading edge suction peaks and high adverse pressure gradients that lead to flow separation. A small degree of roughness needs to be associated with airfoils operating at low *Re* conditions as explained by Lissaman [15] where introduction of 'turbulators' or trip wire devices, promote early transition from laminar to turbulent flow to eliminate laminar separation bubbles and delay the possible chance of separation from the upper surfaces at higher angles of attack. The use of specifically sized trip wires has been employed near the leading edges of high *Re* airfoils to show this effect as studied by Selig and Giguere [10] where the devices 'trip' laminar flow into high energy turbulent flow able to negotiate the APG. Roughness can easily be introduced to airfoils at low *Re* as it does not appear significant in relation to boundary layer thickness whereas the opposite happens at high *Re*. Since boundary layer thickness is inversely proportional to *Re*, a small amount of roughness would appear noticeable with decreasing boundary layer thickness as *Re* is increased since the physical size of the introduced roughness stays the same [3].

Low *Re* airfoils are designed to be thinner than traditional airfoils that operate at high *Re* [7,10,16]. Thin airfoils are chosen for low *Re* application to decrease the suction peak near the leading edge of the airfoil to decrease the APG on the upper surface [13,15]. A decrease in APG ensures that the laminar flow does not separate from the surface. Selig and Giguere [16] discuss the use of thin airfoil that consist of SG60XX series of thin airfoil family (SG6040 – SG6043) suited for application in small wind turbine blades operating in the *Re* range of $1 \times 10^5 - 5 \times 10^5$. Selig and Giguere [10] in another paper discuss the applicability of 15 airfoils consisting of mainly thin airfoil, along the span of

small wind blades. Other geometric optimization such as the increasing of leading edge nose radius and cusping of trailing edge have improved aerodynamic performance at the low *Re*. Increasing nose radius decreases the APG and cusping of trailing edge increases aerodynamic loading within the cusped region [17]. Such airfoils have been proposed for small wind turbines by Selig and McGranahan [18] where of the 6 airfoils that were tested in the *Re* range of 1 x 10^5 – 5 x 10^5, 2 airfoils (SH3055 and FX63-137) were cusped. These airfoils produced C_L values of around 1.8 in the desired *Re* range. Likewise Henriques and Silva [19] developed a new high lift cusped airfoil using Xfoil (T.Urban 10/193) characterized to work well within the urban environment. The airfoil produced C_L values close to 2 in the *Re* range of 6 x 10^4 – 1 x 10^6.

1.4 Small wind turbine rotor blades

Smaller blades with smaller chord lengths combined with low wind conditions leads to the blades operating at low Reynolds numbers from the root to tip [16]. It is vital that small wind turbine rotors have a good startup response to low wind speeds in order to generate maximum possible power [4,10,19]. Most of the starting torque comes from near the blade root whereas the tip generates most of the power producing torque [20]. The starting torque of small wind turbines is small due to their small rotor size deeming it insufficient to start at low wind speeds [7]. Small wind turbines suffer from a lot of resistive torque generated by friction linked to gearbox train, bearings and generator, all of which the rotor has to overcome before it can start rotating. As wind turbines get smaller, cogging friction associated with the generator increases [20]. To overcome this problem, small wind turbines have multiple rotor blades to compensate for the low starting torque [7]. The increased number of blades aid in the quick start of the rotors and allows the turbine to operate at much lower cut-in wind speeds. Although not a good strategy, considering the added cost associated with the extra blades, the cost difference becomes insignificant due to the small size of the turbine [12]. Nevertheless, high performance gains from the wind must be accomplished through aerodynamic optimization of the rotor blades. Aerodynamic optimization of the rotor blades is associated with optimization of the chord and twist distribution, number of blades, choice of airfoil shape, and the tip speed ratio, TSR [21]. With blade optimization, power coefficients close to the Betz limit of 59.2% can be realized for

wind turbines. There is always a trade-off between aerodynamic optimization of the blades and the associated costs, limiting the full potential of aerodynamic optimization as a result of the high cost of production.

Parameters associated with blade geometry optimization are important, because once optimized, shorter rotor blades would produce power comparable to larger and less optimized blades. The efficiency of the rotor largely depends on the blade's profile [6,15] in increasing the lift to generate sufficient torque. As discussed earlier, the airfoil is one of the fundamental parts of a rotor blade design. Its purpose is to induce suction on the upper surface of the blade to generate lift. Drag is also generated perpendicular to the lift and its presence is highly undesirable. In order to maximize the power coefficient and the torque generated, the lift coefficient, C_L and the lift to drag ratio, *L/D* ratio for the airfoil must be maximized [6,22-24]. Higher *L/D* ratios contribute to higher values of torque and it is desirable that at favorable *L/D* ratios, there is maximum C_L in order to have a small sized rotor [15]. Airfoils resistant to laminar flow separation and separation bubbles will greatly improve the performance of small wind turbines without the need for higher rotor solidity. Together with aerodynamic optimization, lighter blades with low rotational inertia would yield better performance at lower wind speeds.

This paper presents the design and performance results of a small horizontal axis wind turbine rated at 400 W with a 1.26 m diameter, 2-bladed rotor designed for low *Re* applications in the wind speed range of 3 – 6 m/s. The blades incorporate twist, taper and a low *Re* AF300 airfoil throughout the blade cross section. The AF300 airfoil was designed to operate in the *Re* range of 0.75 x 10^5 to 2 x 10^5 for application on rotor blades of small wind turbines. The AF300 airfoil has a flatback trailing edge for structural strength and to achieve a higher stalling angle of 14°.

2. Methodology

2.1 Rotor blade design for low wind speed application

A 2-bladed, 1.26 m diameter rotor was designed for low wind speed conditions. The rotor was designed for the Air-X marine wind turbine which has a similar rotor diameter of 1.16 m. The 2-bladed rotor was manufactured from wood to achieve a low rotational inertia for easy start up in low

wind conditions and fiber-coated for stiffness and strength. Taper and twist distributions were incorporated in the design of the rotor. A low Reynolds number airfoil designated as AF300 was specially designed for the rotor blades [25] and formed the basis of the rotor cross-section throughout the span of blades. The AF300 airfoil was tested in the *Re* range of 38,000 – 205,000 corresponding to relative velocities, V_{rel} of 6 – 32 m/s experienced from the root to the tip of the rotor blade. In the *Re* range of 75,000 – 205,000, the AF300 airfoil showed no signs of flow separation up to a stall angle, α_{stall} of 14°, producing C_{Lmax} of 1.72, 1.81 and 1.86 at *Re* = 75,000, 128,000 and 205,000 respectively [24]. Figure 1 shows the geometry of AF300 airfoil.

Flapwise (chord) and edgewise taper distribution and twist distribution for the rotor are shown in figures 2 – 4 based on blade element momentum theory, BEM. Equation 1 gives the chord distribution along the radial distance along the blade span.

$$c(r) = \frac{16}{9} \text{x} \frac{\pi}{4} \text{x} \frac{D^2}{r} \cos^2 \left[\arctan\left(\frac{d}{3\lambda r}\right)\right] \text{x} \left[\frac{1}{\lambda^2 N_b C_L}\right], \quad (1)$$

Where *D* is the overall blade diameter.

r and *d* are the incremental radius and diameter respectivily.

N_b is the number of blades = 2.

λ = 6.5 and C_L =1 [26,27].

The twist distribution based on the *twist of the zero lift line* [28] is shown below in equations 2 and 3:

$$\beta = \left((R\alpha_t/r) - \alpha_t\right) - k(1 - r/R), \quad (2)$$

where β is the pitch angle and α_t is the angle of attack at the tip of the blade:

$$\alpha_t = (\phi - \beta_t) + \alpha_0, \quad (3)$$

α_o is the angle of attack at zero lift and β_t is the pitch angle at the tip ($\beta_t \approx 0°$.)

k is the acceleration factor ($k > 0$)

Figure 3 shows the theoretical pitch distribution based on equation 2 at different values of *k* while figure 4 shows comparison between the twist distribution based on equation 2 at *k* = 0.5 and modified

twist distribution which has pitch angles distributed more evenly along the span of the blade. Figure 5 shows the outline of the rotor blade with taper and twist distribution.

2.2 Rotor specifications

Diameter = 1.26 m

Hub diameter = 0.13 m

Effective rotor radius = 0.565 m

Twist angle, $\beta = 20° – 3° = 17°$

Root and tip pitch angle = 20°and 3° respectively

Rotor solidity, $\sigma = 8.27\%$

Airfoil section = AF300 throughout

Design freestream velocity = 5 m/s

Design rotational speed = 500 rpm

Tip speed ratio, $\lambda = 6.6$

2.3 Passive pitch control

A centrifugal governor was designed to passively govern the pitch of the blades at high rpm as shown in Fig. 6. The governor has masses connected to spring-loaded links that swing in and out depending on the rpm of the rotor. During high rpm, they swing outwards, increasing the pitch angle of the rotor and slowing it down. As rpm decreases, the springs pull back on the links which decrease the pith of the blades. The governor is designed to work when rotor rpm increases above 850 rpm for the purpose of safely braking the rotors. Maximum pitching of 50° is possible during instantaneous braking of the rotors. The governor was constructed on top of the modified custom-designed hub plate to house the 2 blades. The blades are fitted to 8 mm round shaft that rests on ball racer bearing mounts which makes passive pitching and setting the blades at different pitch angles possible.

2.4 Experimental setup for performance testing

The rotor blades were mounted on an Air-X marine turbine from Southwest Windpower, Inc. The electrical power output of the turbine was measured at 3 different pitch angles of 15^o, 18^o and 20° for

performance evaluation in the low wind speed range of 3 – 6 m/s. The Air-X turbine is a 12V DC system capable of producing maximum power of 400 W at 12.5 m/s. It is designed to charge 25Ah – 25000Ah battery banks while an electronic microprocessor controls the charging and electronic braking of the turbine. More information on the turbine is provided in ref. [29].

The turbine was mounted on an 8.22 m tall pole in an open field facing the open ocean at the University of the South Pacific's marine campus. The low-to-strong wind conditions made the site ideal for testing the performance of Air-X wind turbine with the 2-bladed rotor configuration at low wind speeds. Data logging equipment contained inside a monitoring station at the base of the pole recorded average values of wind speed, turbine voltage and current at 10 sec interval at a sampling rate of 1 sec. Data were logged on a CR1000 *Campbell Scientific* data logger. For measuring voltage and current, the logger requires an analog voltage input range of -5 V to +5 V with a resolution of 0.67 μV to 1333 μV. For measuring wind speed, the logger requires a period average input range of -2.5 V to +2.5 V with a maximum measurable frequency of 200 kHz with a resolution of 136ns. Wind speed was measured via a 3-cup A101M anemometer by Vector Instruments which was mounted 1m below the turbine hub and extended 1m horizontally away from the turbine pole. The anemometer can measure a maximum wind speed of 75 m/s with a resolution of 0.1 m/s. Figure 7 shows the setup for the performance testing of Air-X wind turbine with 2-bladed rotor mounted on the 8.22 m pole.

During its operation, the turbine charged a battery bank consisting of deep cycle batteries rated at 12V with a combined load of 200Ah. A voltage regulated load consisting of high wattage filament lamps were connected to the battery bank to provide continual discharge of the battery bank to prevent the wind turbine from shutting down.

3. Results and Discussion

3.1 Performance testing of Air-X wind turbine with the 2-bladed rotor configuration

Data logging of wind speed and turbine's voltage and current output was carried out at 3 different pitch angle settings of 15°, 18° and 20° to find the optimum pitch angle at which the performance is optimum in the low wind speed conditions. Average data values were logged every 10 sec with a 1 sec sampling rate.

Wind turbine power and Coefficient of power, C_p, were evaluated from equations 4 and 5 respectively. For the analysis of power and performance, atmospheric pressure was taken as standard: 101.3 kPa. Ambient temperature was measured at the test site using a portable *Cussons* TA2 hot wire temperature probe. An average temperature value of 25°C was recorded. The air density and temperature are related by the gas equation [9]. The density of air using the gas equation was thus 1.184 kg/m^3.

$$P_T = VI, \tag{4}$$

$$C_P = \frac{P_T}{P_W} = \frac{VI}{\frac{1}{2}\rho A V_\infty{}^3}, \tag{5}$$

Where

P_T is the wind turbine power (W)

V and I are the turbine voltage and current

P_W is the wind power (W)

V_∞ is the freestream velocity of the wind (m/s)

ρ is the density of air (kg/m^3)

A is the rotor swept area (m^2)

3.2 Average power output of Air-X wind turbine with the 2-bladed and the baseline 3-bladed rotor configuration

The power output and performance of the 2-bladed rotor were compared with the 3-bladed stock rotor due to the comparable diameter size (1.26 m vs.1.16 m), rotor solidity (8.27% vs. 8.24%) and low wind speed applications starting from 3-3.5 m/s for the 2 rotors. Average power output was obtained from the scatter plots of power output at different pitch angle setting and collectively plotted together against wind speed to see the effect of pitch angle, β on the power output of Air-X wind turbine. Figure 8 shows the scatter plot of power output of the turbine at β = 18°. Average power output of the Air-X turbine with the baseline (stock) 3-bladed rotor was also compared with the average power output of the 2-bladed rotor (figure

9). The graph shows that maximum power is produced by the 2-bladed configuration at β = 18° followed by 20° and then 15° pitch angles. The Air-X wind turbine outputs similar power at β = 18° and 20° in the wind speed range of 3 - 4.4 m/s. As wind speed increases beyond 4.4 m/s, the rotor set to β = 18° produces more power in comparison to pitch settings of 15° and 20° within the whole wind speed range of interest for the turbine (3-7 m/s). It can be seen that at every given wind speed, the 2-bladed rotor produces maximum power at β = 18°, followed by 20°, 15° and lastly the baseline rotor.

A sound conclusion depends on the turbine's power coefficient C_P to evaluate which rotor configuration performs better. With 8.62% longer blades, the 2-bladed rotor produces more power at all the 3 pitch angles compared to the baseline rotor. At the optimum pitch, β = 18°, the 2-bladed rotor produces more than double the power than the baseline rotor. The power output of the baseline rotor coincides with only 15° pitch setting of the 2-bladed rotor upto a wind speed of 4 m/s.

3.3 Cut-in wind speeds

The average power output graphs show that Air-X starts producing power at cut-in wind speeds of 2.98, 2.34 and 2.38 m/s for β = 15°, 18° and 20° respectively based on instantaneous 10 sec averaged wind speed data. The instantaneous cut-in wind speed was read from the power output graph corresponding to the minimum turbine power. The cut-in wind speeds are presented in table 1 where both instantaneous and averaged cut-in wind speeds, based on average wind speeds corresponding to the minimum power produced were calculated. The averaged value of cut-in wind speed gives a true indication of the turbine's minimum wind speed at which it will start producing power. The turbine will be seen to operate at the instantaneous cut-in wind speed only when it has first started off at the averaged cut-in wind speed and provided that it has gained enough rotational inertia, at which point even if the wind falls below the rated cut-in wind speed, the turbine will still be producing power. Minimum instantaneous and averaged cut-in wind speeds are 2.34 and 3.24 m/s respectivily for the rotors at β = 18°.

3.4 Performance measurements of Air-X wind turbine with the 2-bladed rotor

Figures 11 - 13 show the graphs of maximum, minimum and average C_P variations with the wind speed for 15°, 18° and 20° pitch angles. The maximum, minimum and average C_P variations were plotted from points obtained from the scatter plots of C_P vs wind speed shown in Fig. 10 for β = 18°.

In Fig. 11, the maximum C_P at different wind velocities is plotted for the 3 pitch angles. It is seen that C_P at 20° pitch setting dominates C_P at the other two pitch settings. The turbine performance at β = 20° is marginally better than that at β = 18°. At wind speeds of 5 m/s and above, the C_P of turbine at β = 18° starts to exceed the C_P at β = 20°. In the wind speed range of 4.5 – 6 m/s, C_P ranges from more than 0.2 to around 0.3 for pitch angles of 18° and 20°. At 6 m/s, the power coefficient at β = 18° and 20° pitch angles is close to 0.30 (0.29 and 0.28 respectively).

The variation of minimum C_P with wind speed for the 3 pitch angles is presented in Fig. 12. It can be seen from the graphs that C_P at 18° pitch setting is much higher compared to the other two pitch settings. The performance of the turbine at β = 15° is observed to be marginally better than at β = 20° till a wind speed of 6 m/s. The minimum C_P values reach more than 0.20 after 5.5 m/s for β = 18°. The values of C_P obtained at 6 m/s are 0.24 and 0.20 for β = 18° and 20° respectively.

Figure 13 shows the variation of the average C_P with wind speed for the 2-bladed rotor at different β settings and the 3-bladed baseline rotor. The average performance of the turbine is more important compared to the extreme cases (maximum and mimimum) as it gives a true indication of the turbine's general performance at the respective wind speeds. The turbine has the highest C_p at β = 18°. It is seen that the C_p graphs at β = 18° and 20° coincide with each other up to 4.5 m/s wind speed. Beyond 4.5 m/s, the 18° pitch setting performs better than the other pitch settings. Compared with the performance of Air-X turbine with the baseline rotor, the 2-bladed rotor configuration has better performance at all the pitch settings studied over the wind speed range investigated. The performance curve of Air-X turbine with the baseline rotor matches only with the 2-bladed rotor configuration at β = 15° up to 4 m/s wind speed. Beyond 4 m/s, its C_p values are considerably lower than C_P at β = 15°. The Air-X wind turbine achieves C_P values of more than 0.2 at wind speeds of 5 m/s and above at β = 18° and 20°. At 6 m/s, the turbine attains C_P values of 0.208, 0.255 and 0.24 at the pitch settings of 15°, 18° and 20° respectively whereas with the 3-bladed baseline rotor, the turbine achieves a C_P of

0.15. A small wind turbine was developed and tested by Elizondo et al. [14], but it has rated wind speeds of about 10 m/s. The present work addresses and solves some of the technological issues associated with small wind turbines raised by Clausen and Wood [7].

3.4 Operation of the 2-bladed rotor at high wind speeds

The Air-X marine wind turbine comes with a microprocessor that limits the rotors' rpm to 850 rpm in high wind speeds [**30**] with the power producing rpm ranging between 500 – 850 rpm [**29**]. The turbine will stall the rotor at $V_\infty > 15.6$ m/s and completely shut it down at $V_\infty > 22$ m/s to protect both the rotor blades and the generator. Since the 2-bladed rotor produces more power compared to the baseline rotor at the same wind speeds, it rotates at a higher rpm and with more torque which increases the thrust and the centrifugal force on the blades at a lower wind speed compared to the baseline rotor. The 2-bladed rotor is thus constructed from wood, clothed in fiberglass for strength and stiffness. Together with this, the flatback trailing edge and cusped shape of the airfoil adds strength and rigidity so that the blades don't easily bend due to the thrust caused by strong winds. With small wind turbines, the effect of thrust is minimized by the high rotation that the rotor goes through; the high rpm of the blades induces a very strong centrifugal force causing the blades to be stiff and maintain parallelism with the rotor plane of rotation.

As discussed in section 2.3, a custom-built centrifugal governor was employed to safeguard the rotor in case the turbine's active braking fails. Figure 14 shows the graph of pitch angle vs. governor rpm. It shows an exponenital increase in pitch angle whereby β increases abruptly from 881rpm and is fully 'braked' at 1020 rpm which takes a fraction of a second due to the rapid dispalcement of the governor masses from the middle to the outermost positions on the governor arms to increase the centrifugal force to instantly brake the rotors.

During rpm regulation, rpm of the rotor will cycle to the specific rpm from the operating rpm range (500 – 850rpm) at which the system should be generating electrical power. The cycle is sinusoidal because of the balancing effect of the masses and governor arm retainer springs which pull on the governor arms to a closed position after the rotor has slowed down through pitch regulation.

4. Conclusions

A 2-bladed rotor was designed to work with the Air-X wind turbine to operate in low wind speed conditions that are present in the Pacific Island Countries. The cross section of the blades consisted of AF300 flatback airfoil, specially designed to achieve high lift at low Reynolds numbers and provide structural stability to the blades. The added structural strength as a result of the flatback trailing edge meant that the blades could be made from even lighter materials benefiting the rotor with low inertia and resulting in lower startup and cut-in wind speeds.

The 2-bladed rotor was manufactured from wood to be light and designed to operate in wind speed range of 3 – 6 m/s. The rotor incorporated an exponential twist and taper distribution and the AF300 airfoil for increased aerodynamic performance at low wind speeds. The chord distribution of the blades resulted in the outer portion to have higher solidity compared to the baseline blades to have a fast start up and low cut-in wind speed.

The turbine was field tested at 3 different pitch angles of 15°, 18° and 20°, with the turbine performing best at 18°. The 2-bladed rotor recorded instantaneous and average cut-in wind speeds of 2.34 m/s and 3.24 m/s respectively, compared to the cut-in wind speed of 3.58 m/s measured for the rotor with the baseline blades. Performance of Air-X with the 2-bladed rotor was compared to the baseline rotor and found that the 2-bladed rotor has better C_P in the low wind speed range of 3 – 7 m/s. The 2-bladed rotor achieved C_P values of 0.l, 0.217 and 0.255 at the wind speeds of 4, 5 and 6 m/s respectively wherease the baseline 3-bladed rotor achieved 0.052, 0.112 and 0.15 at these wind speeds. Peak power coefficient attained by the 2-bladed rotor design at 6 m/s wind speed was 0.29.

References

[1] Cooper P, Kosasih PB, Ledo L. Roof mounting site analysis for micro-wind turbines. Renewable Energy 2010; 36:1379-1391.

[2] Hirahara H, Hossain MZ, Nonomura Y. Testing basic performance of a very small wind turbine designed for multi – purposes. Renewable Energy 2005; 30: 1279 – 1297.

[3] Fasel HF, Gross A. Numerical Investigation of Different Wind Turbine Airfoils. The University of Arizona, Tucson, Orlando, Florida; 2011.

[4] Ozgener O, Ozgener L. Exergy and reliability analysis of wind turbine systems: a case study. Renewable and Sustainable Energy Reviews 2007; 11:1811–1826.

[5] Wang F, Bai L, Fletcher J, Whiteford J, Cullen D. The methodology for aerodynamic study on a small domestic wind turbine with scoop. Wind Engineering and Industrial Aerodynamics 2008; 96:1–24.

[6] Mayer C, Bechly ME, Hampsey M, Wood DH. The starting behaviour of a small horizontal-axis wind turbine. Renewable Energy 2001; 22:411-417.

[7] Clausen PD, Wood DH. Research and development issues for small wind turbines. Renewable Energy 1999; 16:922-927.

[8] Peacock AD, Jenkins D, Ahadzi M, Berry A, Turan S. Micro wind turbines in the UK domestic sector, energy and buildings. Renewable Energy 2008; 40:1324–1333.

[9] McGranahan BD, Selig MS. Wind Tunnel Aerodynamic Tests of Six Airfoils for Use on Small Wind Turbines. National Renewable Energy Laboratory, Colorado; 2004.

[10] Giguere P and Selig MS. Low reynolds number airfoils for small horizontal axis wind turbines. Wind Engineering 1997; 21:379.

[11] Hall J, Mohseni K, Sahin M. Direct Numerical Simulation of Separated Low-Reynolds Number Flows around an Eppler 387 Airfoil. Department of Aerospace Engineering Sciences, University of Colorado, Boulder, Colorado; 2007

[12] Mayer C, Bechly ME, Hampsey M, Wood DH. The starting behaviour of a small horizontal-axis wind turbine. Renewable Energy 2001; 22:411-417.

[13] Miley SJ. A catalog of low reynolds number airfoil data for wind turbine applications. Department of Aerospace Engineering Texas A&M University College Station, Texas; 1982.

[14] Elizondo J, Martinez J, Probst O. Experimental study of a small wind turbine for low- and medium-wind regimes. International Journal of Energy Research 2009; 33: 309-326.

[15] Lissaman PBS, Low-Reynolds-Number Airfoils. Annual Reviews of Fluid Mechanics 1983; 15:223-239.

[16] Giguere P, Selig MS. New airfoils for small horizontal axis wind turbines. Wind Engineering 1998; 120:111.

[17] Anderson JD, Fundamentals of aerodynamics. 3rd ed. New York: McGraw Hill; 2001.

[18] McGranahan BD, Selig MS. Aerodynamic Tests of Six Airfoils for Use on Small Wind Turbines. University of Illinois at Urbana-Champaign Urbana, Illinois; 2004.

[19] Henriques JCC, Silva M, Estanqueiro AI, Gato LMC. Design of a new urban wind turbine airfoil using a pressure-load inverse method. Renewable Energy 2009; 34:2728–2734.

[20] Wright AK, Wood DH. The starting and low wind speed behavior of a small horizontal axis wind turbine. Wind Engineering and Industrial Aerodynamics 2004; 92:1265–1279.

[21] Badr MA and Maalawi KY. A practical approach for selecting optimum wind rotors. Renewable Energy 2003; 28:803–822.

[22] Lanzafame R and Messina M. Design and performance of a double-pitch wind turbine with non-twisted blades. Renewable Energy 2009; 34:1413–1420.

[23] Guglielmo JJ, Selig MS. High-lift low Reynolds number airfoil design. Journal of Aircraft 1997; 34.

[24] Ahmed, MR. Blade sections for wind turbine and tidal current turbine applications – current status and future challenges. International Journal of Energy Research 2012; 36: 829-844.

[25] Singh RK, Ahmed MR, Zullah MA, Lee YH. Design and testing of a low Reynolds number airfoil for small horizontal axis wind turbines. Renewable Energy 2012; 42: 66-76.

[26] Hau E. Wind Turbines – Fundamentals, Technologies, Application, Economics. 2 ed. United Kingdom: Springer; 2006.

[27] Lanzafame R, Messina M. Power curve control in micro wind turbine design. Energy 2009; 1 – 6.

[28] Habali SM, Saleh IA. Local design, testing and manufacturing of small mixed airfoil wind turbine blades of glass fiber reinforced plastics Part I: design of the blade and root. Energy Conversion & Management 2000; 41:249-280.

[29] Air-X owner's manual, Southwest Windpower, Inc. Flagstaff, Arizona; 2008.

[30] Dam JV, Migliore P, Meadors M and Link H. Power Performance Test Report for the Southwest Windpower AIR-X Turbine. National Renewable Energy Laboratory, Colorado; 2003.

Nomenclature

A rotor swept area (m^2)

C_L coefficient of lift (dimensionless)

C_{Lmax} maximum coefficient of lift at stalling angle (α_{stall}) (dimensionless)

C_D coefficient of drag (dimensionless)

C_P coefficient of power (dimensionless)

L/D lift to ratio (dimensionless)

Re $\rho V_\infty c/\mu$, Reynolds number (dimensionless)

V_∞ freestream velocity (m/s)

V_{rel} relative velocity (m/s)

α_{stall} stalling angle of attack where maximum value of lift coefficient occurs

λ tip speed ratio (TSR) (dimensionless)

ρ density of air (kg/m^3)

β angle measured between the rotor plane of rotation and chordline of airfoil section at the root of rotor blade (°)

List of figures

Fig. 1 The profile of Airfish AF300 airfoil

Fig. 2 Flapwise and edgewise taper distribution along the rotor radius

Fig. 3 Blade twist distribution based on the twist of zero lift line equation

Fig. 4 Modified blade twist distribution compared with twist of zero lift line equation with $k = 0.5$

Fig. 5 Schematic diagram of the 2-bladed rotor blades

Fig. 6 Photograph of the custom-made hub plate and centrifugal pitch control governor

Fig. 7 Close-up view of the Air-X turbine with the 2-bladed rotor and anemometer setup

Fig. 8 Scatter plot of power output at the optimum pitch angle of 18 degrees

Fig. 9 Average power output of the turbine at different wind speeds and different pitch angles. The power output of the rotor with baseline blades is also shown

Fig. 10 Scatter plot of the power coefficient at the optimum pitch angle of 18 degrees

Fig. 11 Maximum power coefficient of the turbine as a function of wind velocity at different pitch settings

Fig. 12 Minimum power coefficient of the turbine as a function of wind velocity at different pitch settings

Fig. 13 Average power coefficient of the turbine as a function of wind velocity at different pitch settings. Also shown is the power coefficient of the rotor with baseline blades

Fig. 14 Blade pitch angle (β) vs. rotational speed of the centrifugal governor for pitch angle setting of 20 degrees

List of tables

Table 1 Cut-in wind speeds for Air-X turbine with the designed 2-bladed rotor

Table 1

Pitch angle setting (°)	Instantaneous cut-in wind speed (m/s)	Averaged cut-in wind speed based on minimum power output (m/s)
15	2.98	3.46
18	2.34	3.24
20	2.38	3.33

Table 1 Cut-in wind speeds for Air-X turbine with the designed 2-bladed rotor

Figure 1

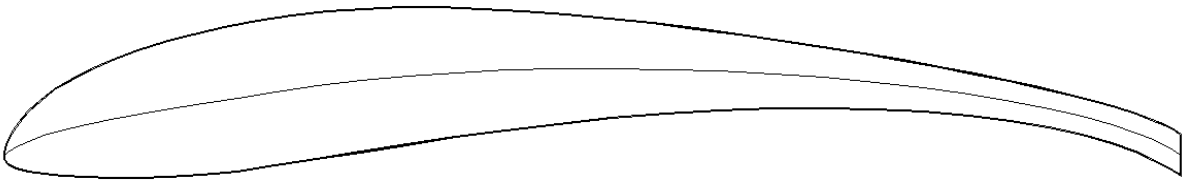

Fig. 1 The profile of Airfish AF300 airfoil

Figure 2

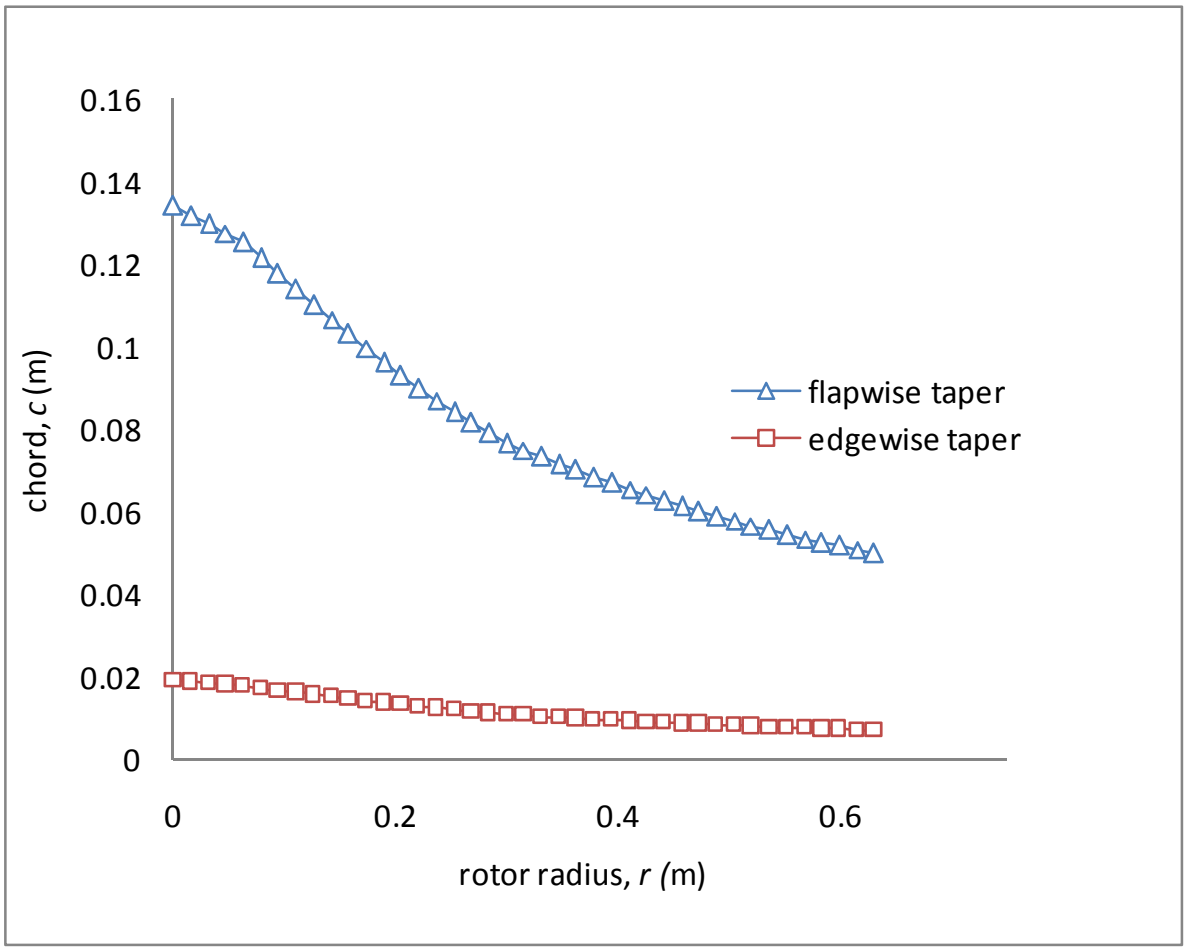

Fig. 2 Flapwise and edgewise taper distribution along the rotor radius

Figure 3

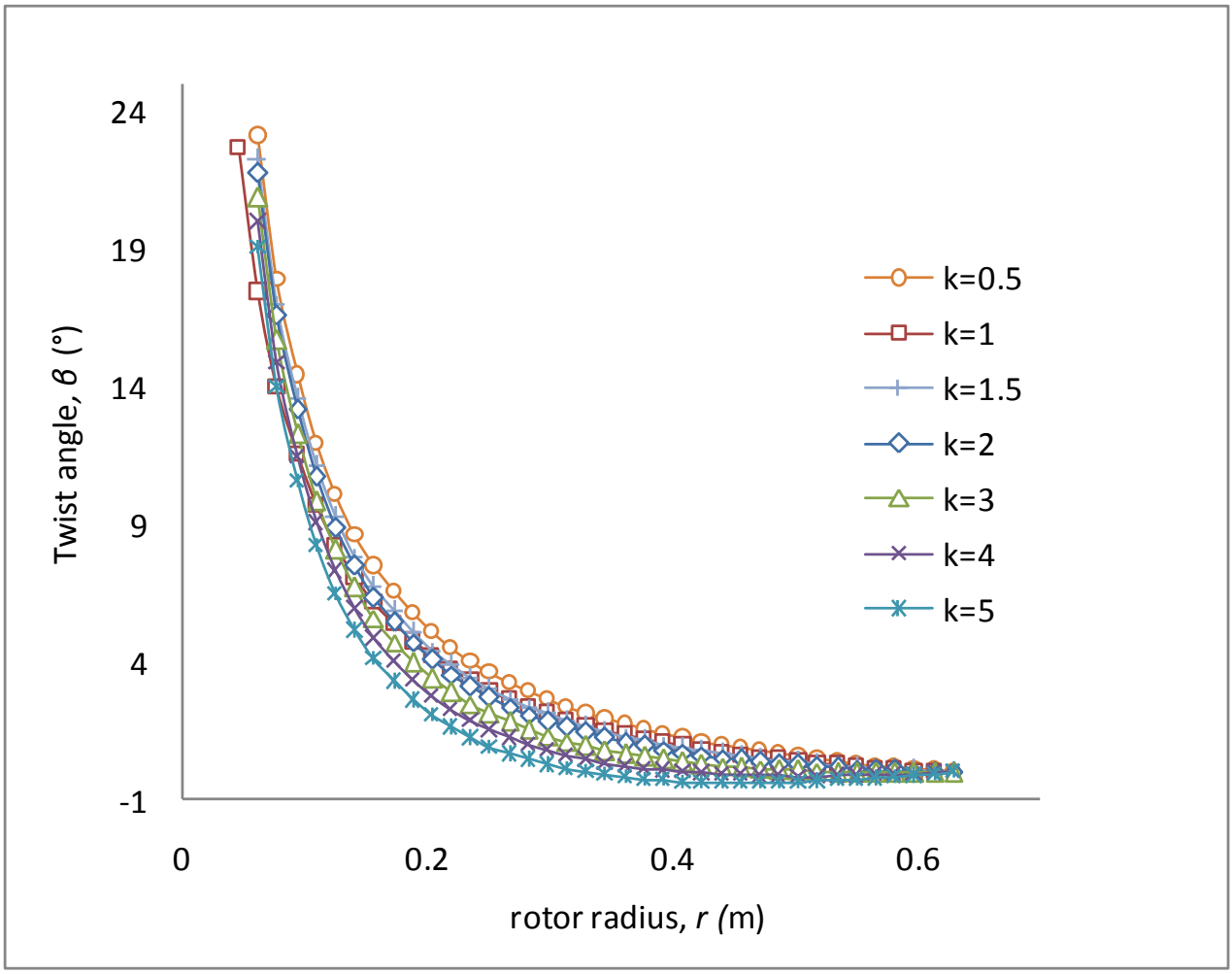

Fig. 3 Blade twist distribution based on the twist of zero lift line equation

Figure 4

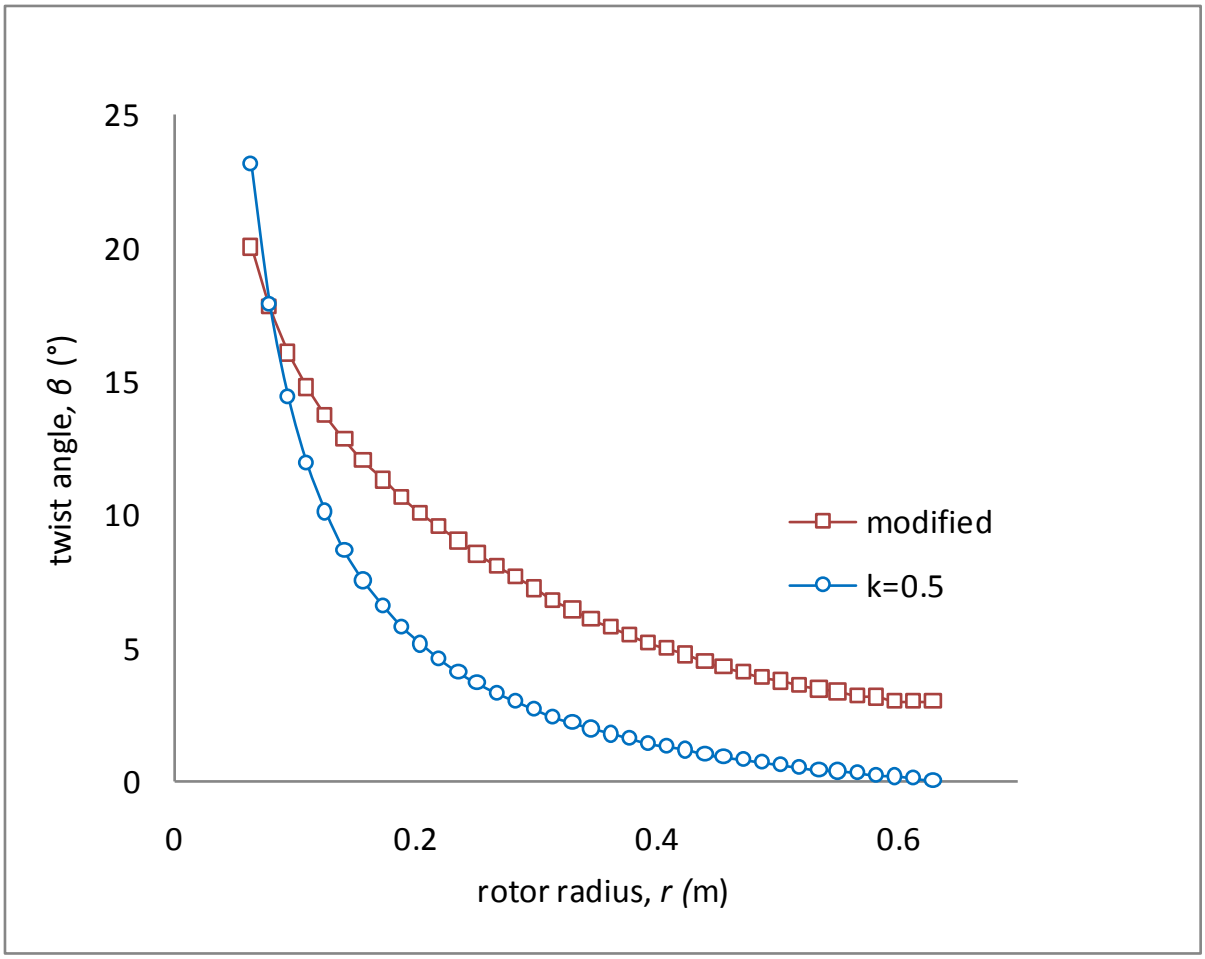

Fig. 4 Modified blade twist distribution compared with twist of zero lift line equation with $k = 0.5$

Figure 5

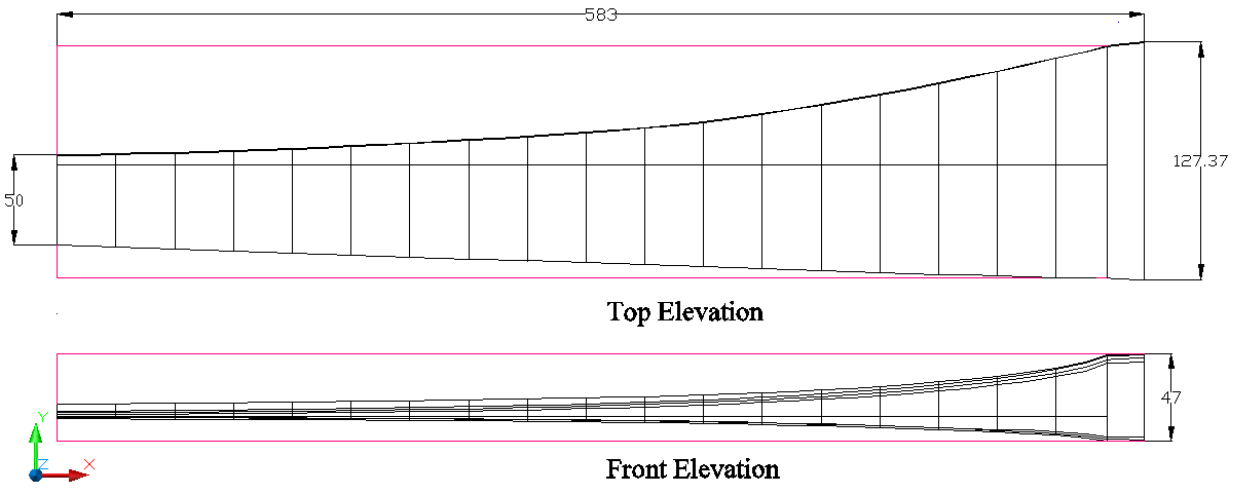

Fig. 5 Schematic diagram of the 2-bladed rotor blades

Figure 6

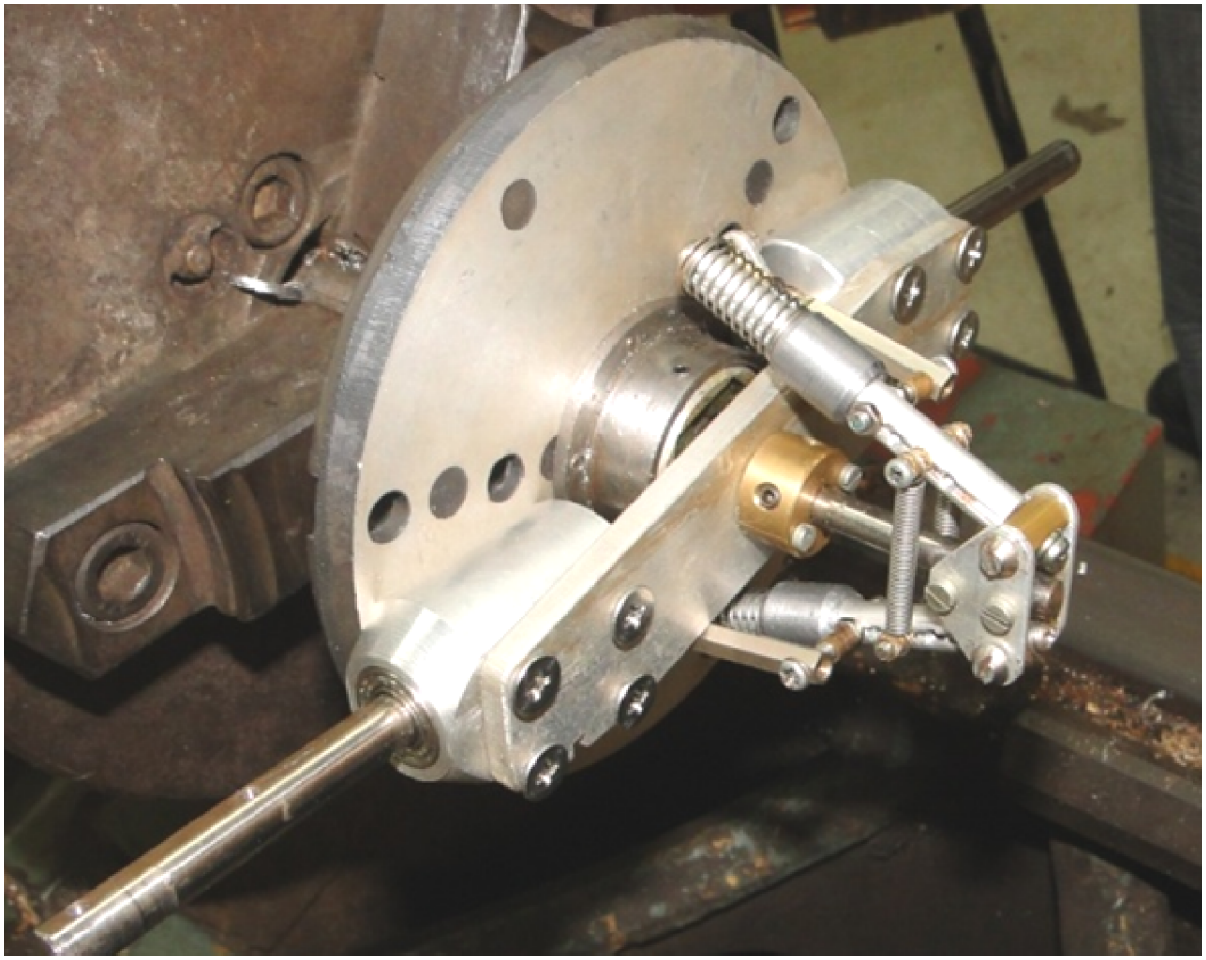

Fig. 6 Photograph of the custom-made hub plate and centrifugal pitch control governor

Figure 7

Fig. 7 Close-up view of the Air-X turbine with the 2-bladed rotor and anemometer setup

Figure 8

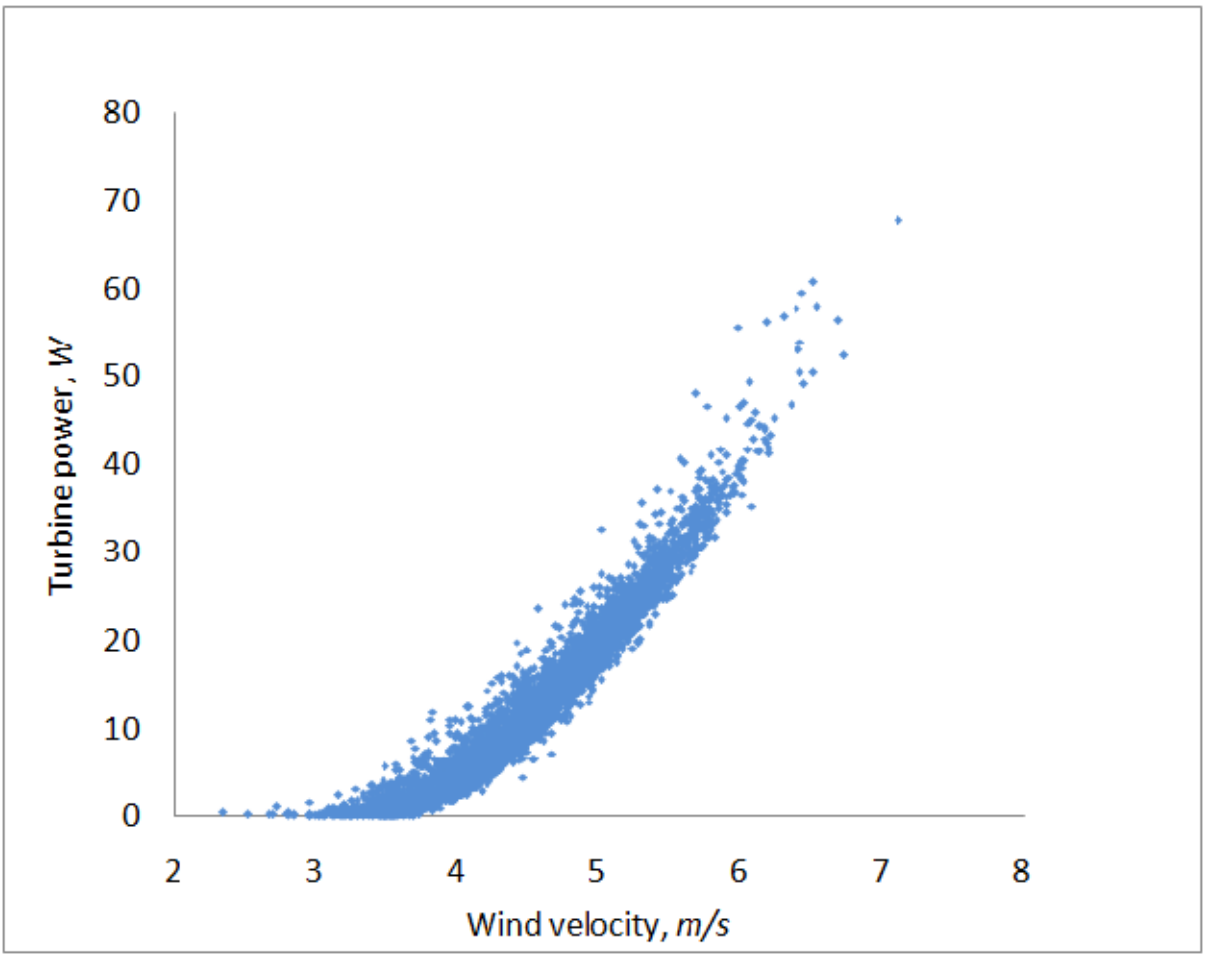

Fig. 8 Scatter plot of power output at the optimum pitch angle of 18 degrees

Figure 9

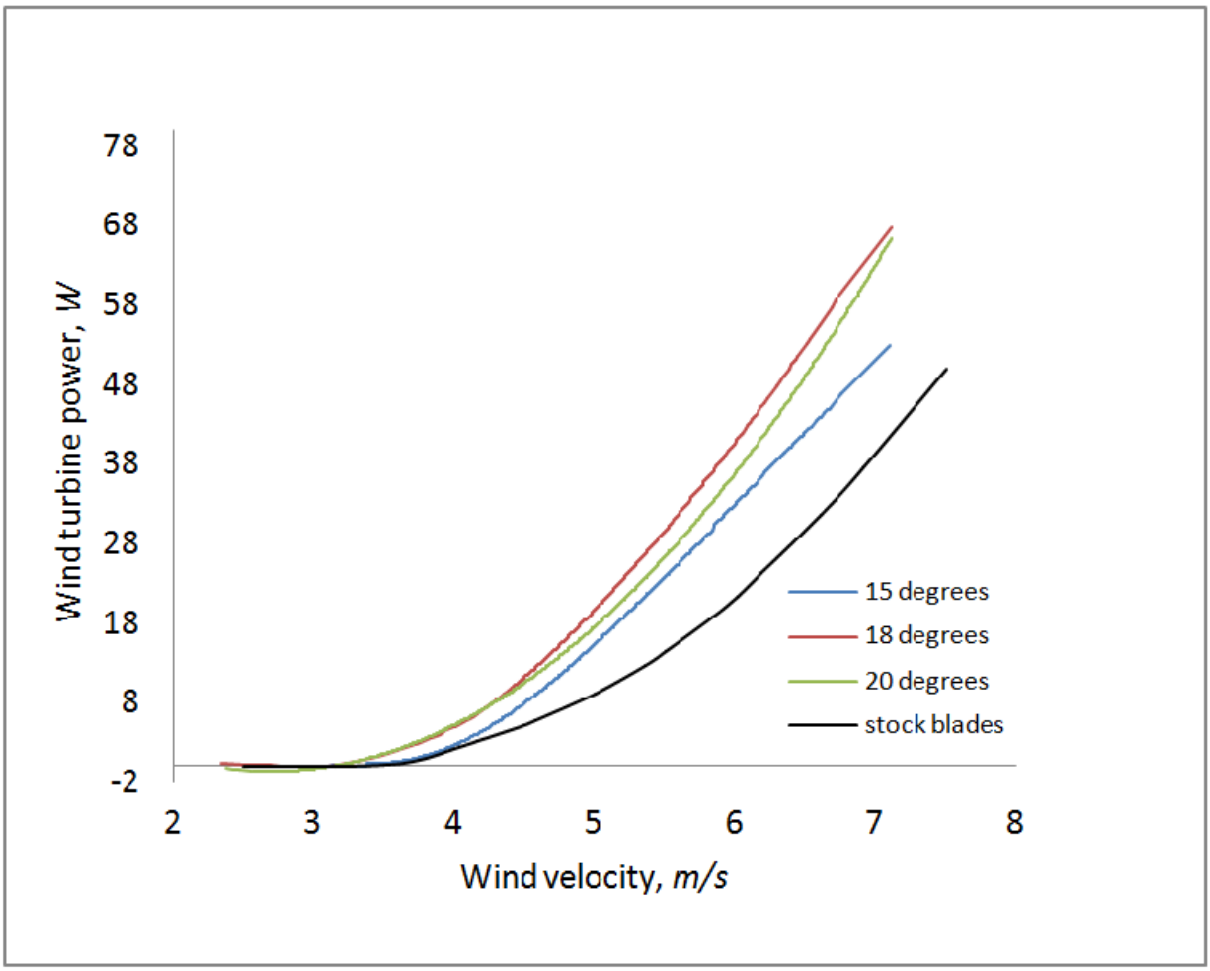

Fig. 9 Average power output of the turbine at different wind speeds and different pitch angles. The power output of the rotor with baseline blades is also shown

Figure 10

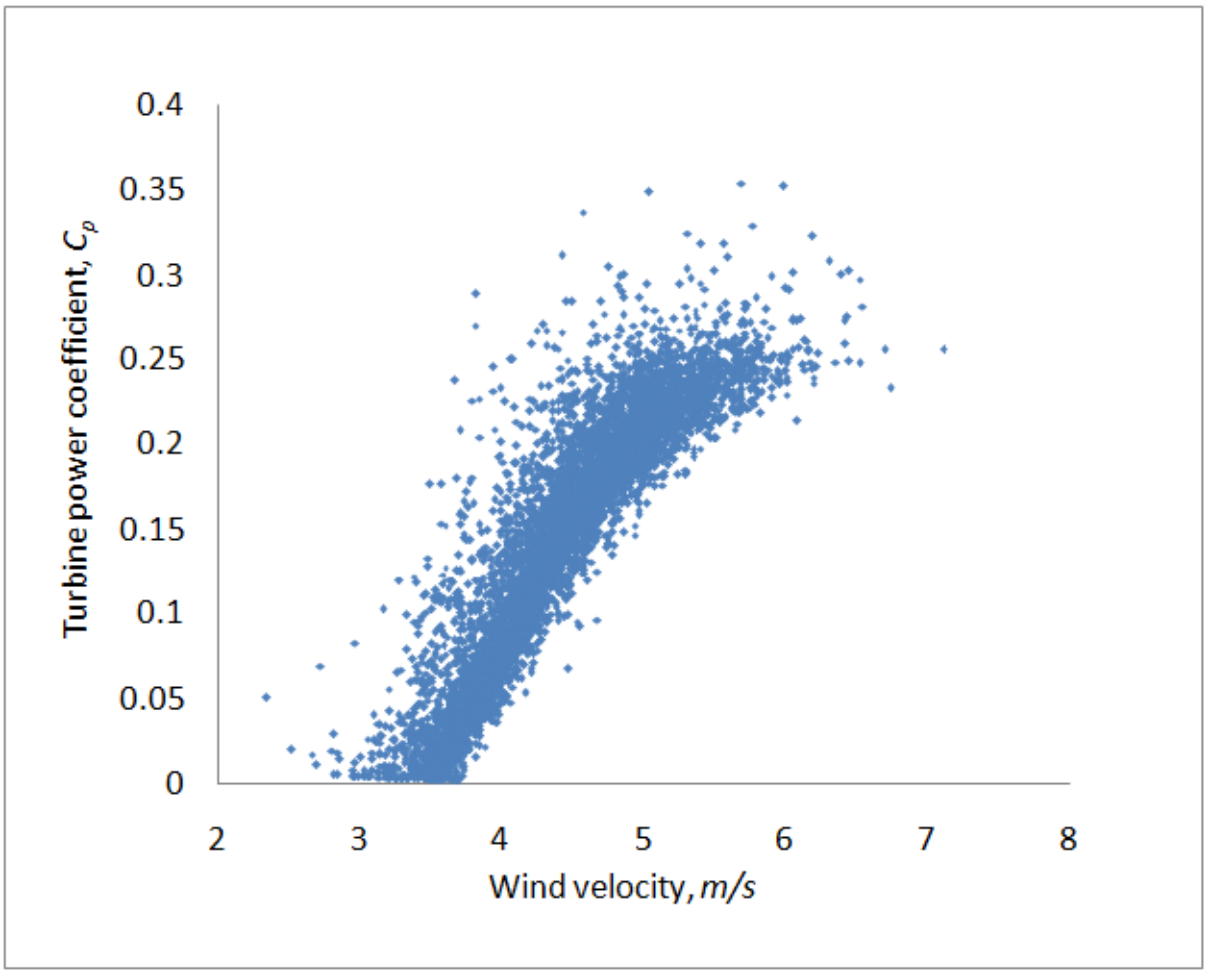

Fig. 10 Scatter plot of the power coefficient at the optimum pitch angle of 18 degrees

Figure 11

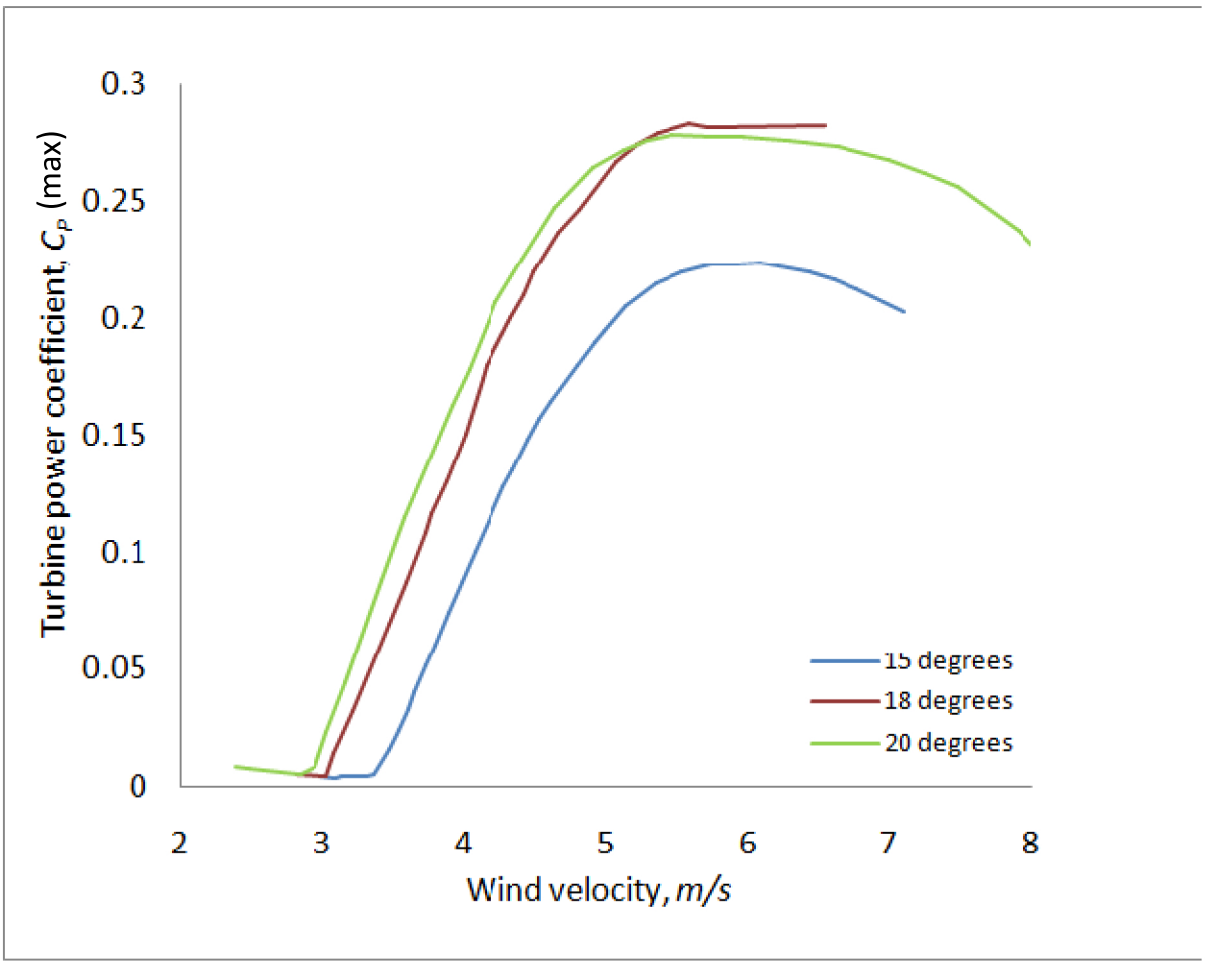

Fig. 11 Maximum power coefficient of the turbine as a function of wind velocity at different pitch settings

Figure 12

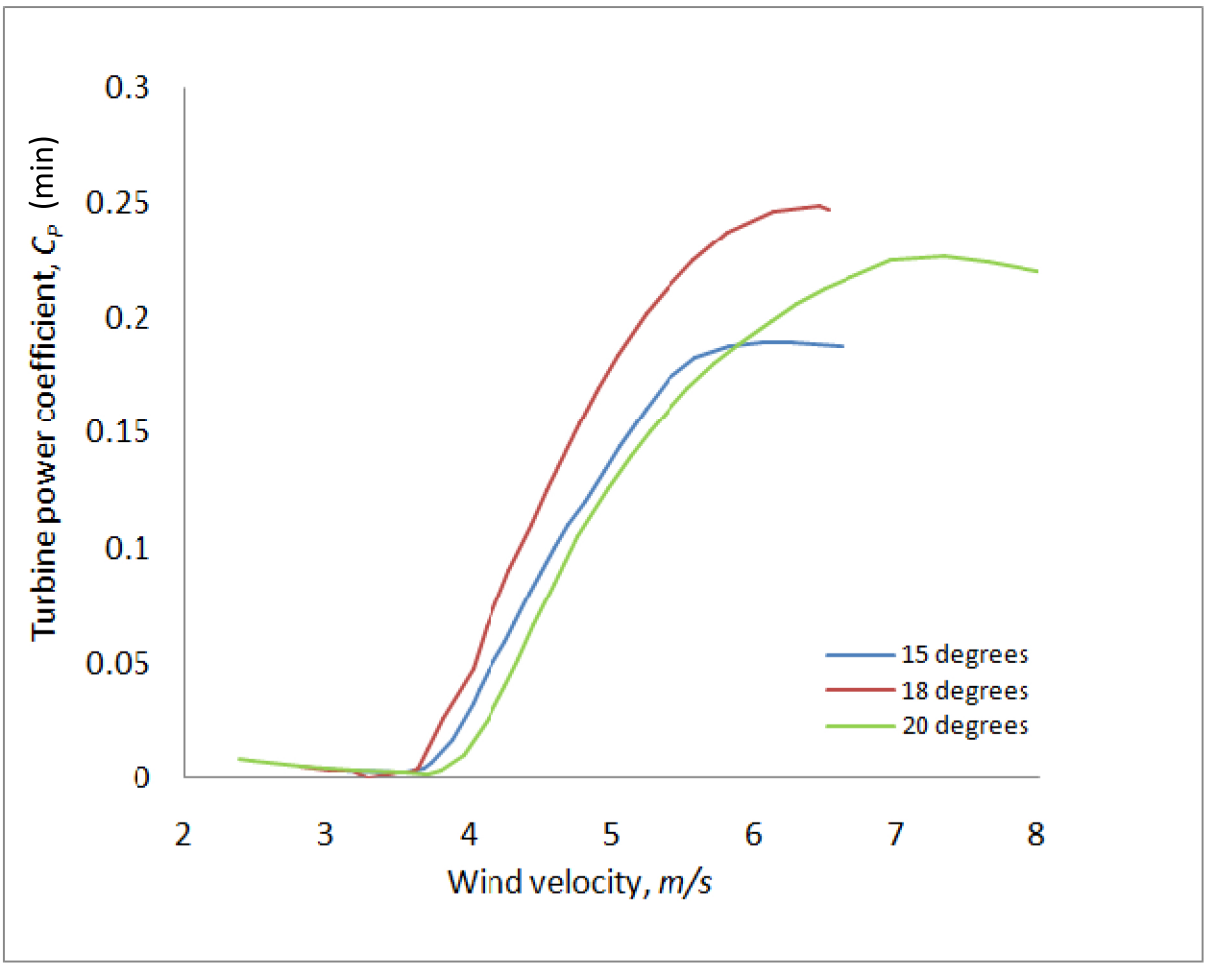

Fig. 12 Minimum power coefficient of the turbine as a function of wind velocity at different pitch settings

Figure 13

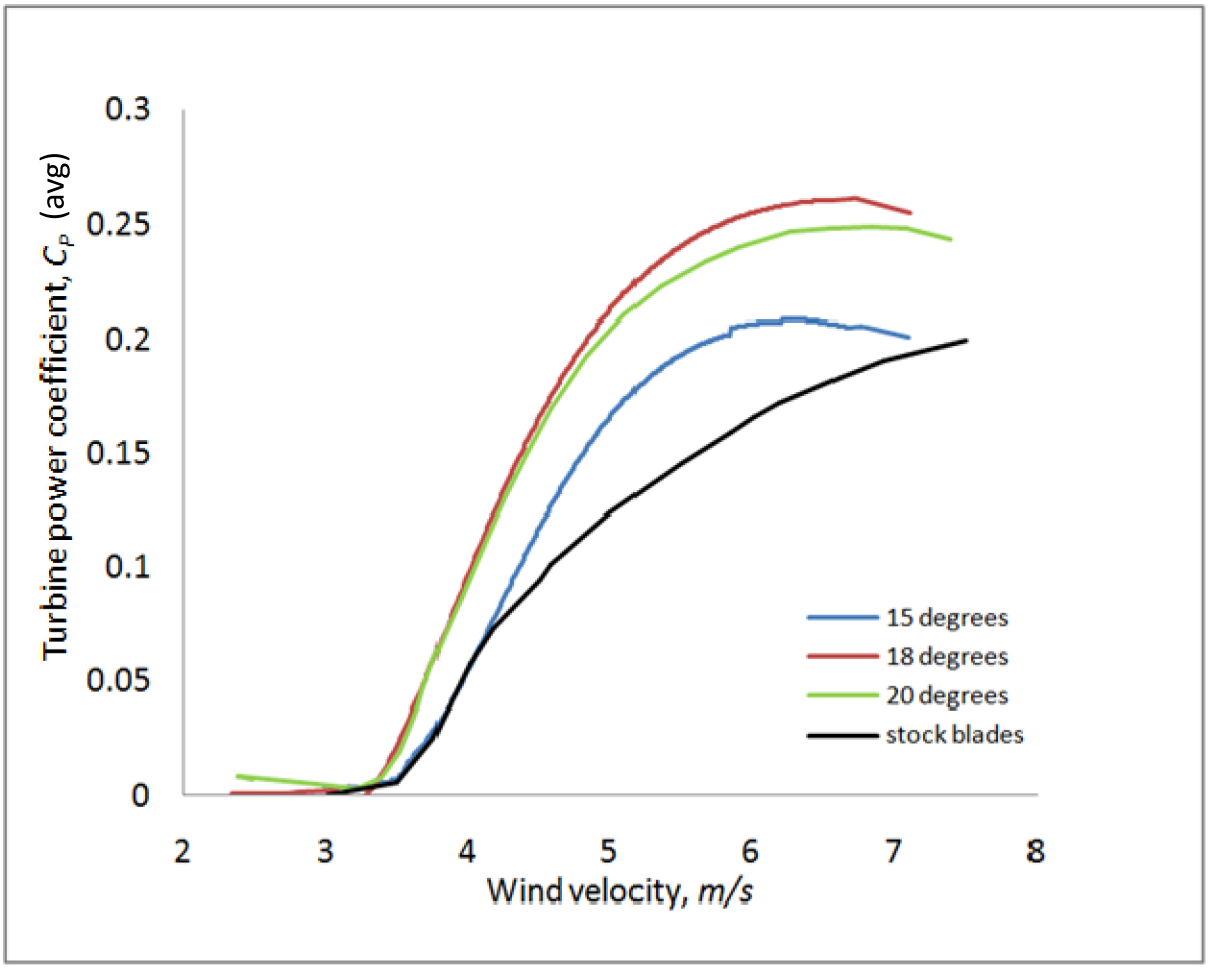

Fig. 13 Average power coefficient of the turbine as a function of wind velocity at different pitch settings. Also shown is the power coefficient of the rotor with baseline blades

Figure 14

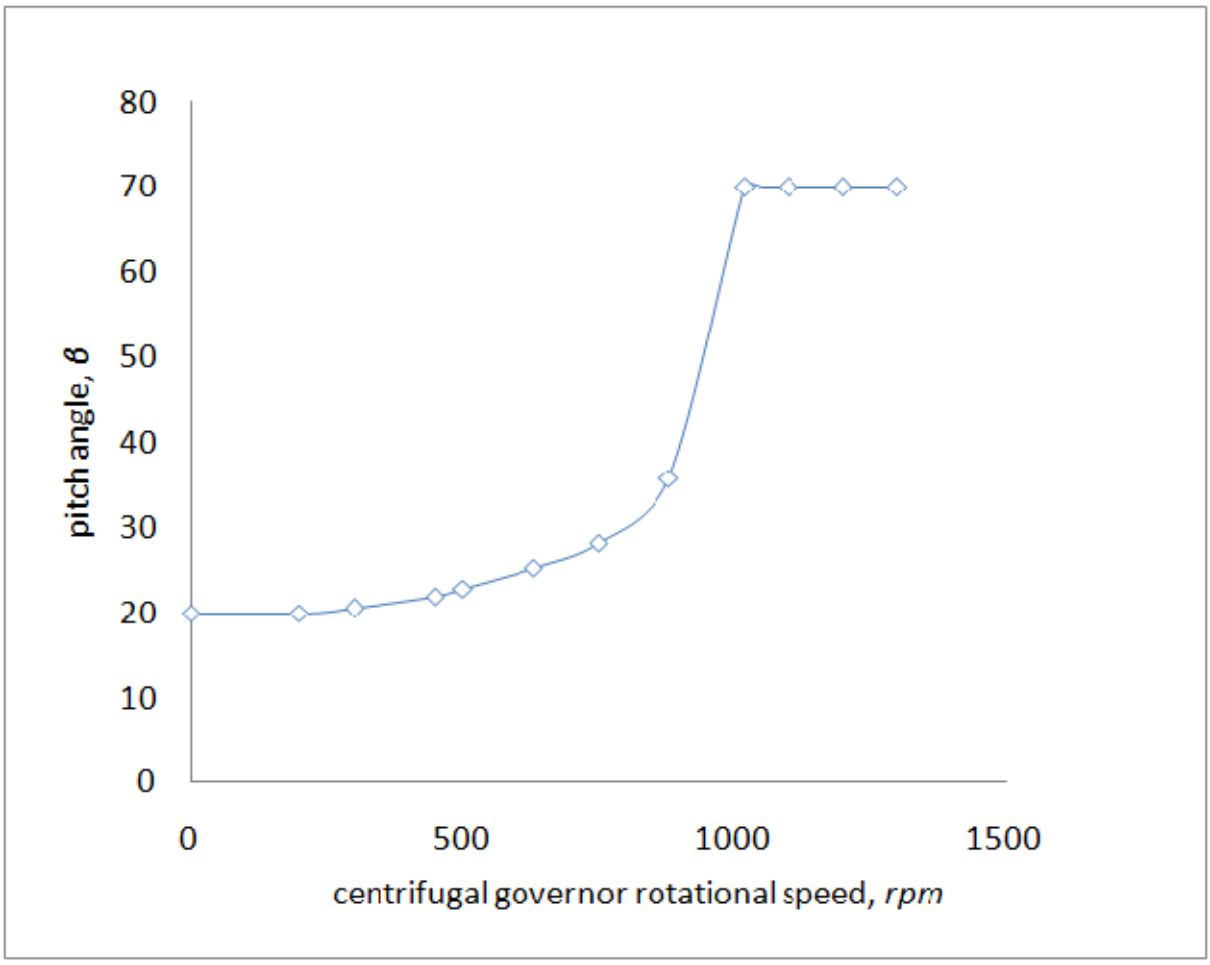

Fig. 14 Blade pitch angle (β) vs. rotational speed of the centrifugal governor for pitch angle setting of 20 degrees